Metallographic Characterization of SiC-Ni-Ti Layer Reinforced on Austenitic Stainless Steel (AISI 316L) by Two-step Laser Fabrication

C. Ramesh Kannan (crkannanmech@gmail.com)
Dr Navalar Nedunchezhiyan College of Engineering
S. Manivannan
Karpagam Academy of Higher Education: Karpagam University
B. Stalin
Anna University of Technology Madurai
C. Kailasanathan
Sethu Institute of Technology

Research Article

Keywords: Ceramic, Laser cladding, MMC, SiC-Ni-Ti, AISI316, Metallographic characterization

Posted Date: May 26th, 2021

DOI: https://doi.org/10.21203/rs.3.rs-524562/v1

Version of Record: A version of this preprint was published at Silicon on August 17th, 2021. See the published version at https://doi.org/10.1007/s12633-021-01305-y.

Abstract

Industry X.0 is the new paradigm that is the driving phenomenon in the process of making things and the new method in which they are produced. In this work, we attempt to fabricate ceramic layer reinforced metal matrix composite (MMC) of AISI 316L by a two-step laser process. Coatings of metal-ceramic powders of 40% SiC-40%Ti-20% Ni and 60% SiC-30%Ti-10% Ni was preplaced on 316L specimens. High power laser was used to irradiate the preplaced coatings to form MMCs of metal-ceramic particles. The composition of the MMC layer was studied by using optical emission spectroscopy (OES) and its microstructure of the MMC layers, phase analysis and its elemental analysis were characterized by optical and scanning electron microscopy (SEM), X-ray diffractometry, and image analyzing techniques, respectively. The results confirmed that due to the formation of non-uniformity of coating thickness, microporous and crack formation at layer of MMC, revealed that a higher percentage of ceramic particles present in the MMC layer entails a particular disadvantage.

1. Introduction

The present global scenario is moving towards swift, exponential, and continuous change. Besides, the industrial revolution cannot be an alternative for addressing this change. Therefore, an entire renovation in a digital sense is required in the process of making things and also the things that are made. Moreover, this new trend is known as Industry X.0 [1]. Further, this renovation achieved through Industry X.0 is matchless and might also aid the manufacturing and production houses to imbibe the change. Hence, this paradigm might create a platform for manufacturing businesses to accomplish greater success in the changing world.

Due to the corrosion resistance property of AISI316L, it is widely deployed in the petrochemical industry and refineries [2]. However, AISI316L stainless steel life is critical due to its relatively weak wear resistance. The improvement of wear resistance at the matrix is due to the overlaying of the dispersion of very hard and fine ceramic particles into AISI316L [3]. Segregation (micro/macro) as non-uniform distribution of particles is difficult to achieve through the melting and casting route. Further, the smaller component is manufactured through the powder metallurgical route. The source of heat used was a high beam process like laser/EBW over-layering to melt material in the form of powders painted over the surface of substrates and subsequently building the layer [4].

The potential benefits of using laser cladding are enormous than conventional techniques. Few are faster speed, cleanliness, favourable heating/cooling rate, and ease of solidification [5]. It has been conveyed that the technique of direct laser cladding was applied for Ti-based alloys and stainless steels [6–9]. Although, this technique has not been applied for synthesizing metal matrix composite (MMC), except by Wang et al. [10]. They have reported that the development of Ti-6Al-4V MMC. Further, for improving wear resistance, simultaneous application of laser surface alloying and cladding has been applied to metallic materials [11–13]. In this research work, AISI316L stainless steels were developed and dispersed layers were characterized. Furthermore Vickers micro-hardness was measured.

2. Materials And Methods

As the substrate, AISI 316L stainless steel (size: 100 x 100 x 5 mm^3) was taken, and the surface was cleaned by acetone. Table 1 presents the chemical composition of AISI 316L stainless steel, which is confirmed by optical emission spectroscopy (OES) technique, Test Point, Coimbatore, Tamil Nadu, India. Through the mixture of pre-alloyed powders of SiC, Ti, and Ni with polyvinyl alcohol glue, the coating was done by painting on the substrate. The coatings thickness was measured as 500 microns, and the particle size for the powders has been measured about 320 mesh sizes. Further, the coating was dried at room temperature, and it was irradiated with a 5kW CW CO_2 laser. During cladding, Argon gas was used to prevent the oxidation of the melt pool. Table 2 represents that the process parameters were used for the present investigation.

Table 1
The chemical composition of authentic stainless steel (SS316L).

Elements	C	Cr	Ni	Mo	Mn	Si	P	S	Fe
wt%	0.028	18.12	10	2.5	2.0	0.75	0.038	0.003	Balance

The microstructure of the laser-treated surface was characterized by using optical and scanning electron microscopy techniques. For two minutes, the samples were mirror polished and electrolytically etched with 10% oxalic acid at 6 Volts. The microhardness tester with a load of 100grams for 15seconds dwell time, the microhardness of the samples was measured by using Shimadzu HMV-2T. The XRD phase evolution during laser treatment was analyzed by using Rigaku Ultima III XRD The phase formation and XRD and EDS analysis confirmed elemental compositions. Figure 1 show that the excitation source has emitted continuously from flash lamps and reflected through the rear and front mirror. The continuous action of the emitting laser was focused on using the lens and concentrated on the particular workpiece. The emitting energy is mainly focused on the workpiece through a particular lens, and it was melted with the help of temperature sourced from the origin of the Nd YAG source. During the melting of the workpiece, a sufficient amount of argon was supplied in the melt zone area for avoiding oxidation from the environment. Simultaneously, it was recorded through the temperature and force load sensor. The signal was analyzed and contained at each and every stage of the location of the workpiece movement with respective temperature and load sensors. Finally, it was indicated with the help of the computer record.

Table 2
The processing parameters used for laser coating.

Specimen Q (40wt% SiC – 40wt% Ti – 20wt% Ni)	Specimen K (60 wt% SiC – 30 wt% Ti -10 wt% Ni)	Laser power (kW)	Laser scanning speed (mm/min)	Beam diameter (mm)	Energy density E = q/(vxd) (J/mm^2)
Q1	K1	2.0	1.0	2	35
Q2	K2	2.0	2.0	2	30
Q3	K3	1.5	2.0	2	23

3. Results And Discussion

3.1. Microstructural analysis

Figure 2 shows the optical microstructures of the laser-treated samples. The surface morphology of the laser-treated zone differs; depends upon parameters and the composition of the SiC-Ti-Ni was indicated by the microstructures. The microstructure of the laser-treated region for samples Q1, Q2, and Q3 (Fig. 2) shows a smooth surface with uniform melting and distribution of powders. It is observed that laser melted regions show two different microstructural characteristics; one is intensely bright layers shown in Fig. 2a and the other one is white layer appears over the dark layer with low intensity is shown in Fig. 2b. The energy density of 30–40 J/mm^2 leads to the formation of a dark layer. The microstructure reveals homogeneous clad with crack-free and less porosity. A good bonding was achieved between the clad surface and substrate which attributes to the selection of process parameters for the above samples.

The microstructure of samples K is shown in Fig. 3. It reveals that for samples K1, K2, and K3, by a significant amount of porosity, roughness, and surface irregularity the clad layer is characterized due to excessive porosity and brittleness. The spilling of the alloyed region in the clad surface also observed, which leads to residual thermal stresses generated, the coefficient of low thermal expansion on the substrate, and the alloying powder was responsible for the poor cladding of the surface.

3.2. Microhardness testing

Overall, Vickers microhardness was measured; values were obtained between 1300 HV. Specific factors include the transformation characteristics of the material and the relative amount of the phases present and changes in the process parameters, which will contribute to the overall heat input which will control the cooling rate. The interface region exhibited lower hardness, principally attributed to re-melted and re-heated at least twice; this will give a tempering effect on the material which plays a role in reducing the hardness. The metal becomes softer towards the metal substrate, and the material is hardest at the top surface. The region near the substrate is softer than the top layers because they had a more extended temperature history, as layers of cladding were added to the sample, the previous layer was heated up

again which will result in the superimposition of the heat this will increase the overall heat input, this reduces the cooling rate effectively. An improvement in the surface hardness of 316L was achieved.

3.3. Scanning electron microscopy analysis

In general, Fig. 4 shows the microstructure of the cross-sectional laser cladding of specimen Q1 with a laser scanning speed of 2 m/min and 2 kW (laser power). It is concluded that the clad layer is about 380 μm thick and it shows that there are no pores and cracks. A strong adhesive between the laser clad layer and substrate is observed. The samples Q2 and Q3 also exhibit similar behaviour other than a few cracks.

When SiC-Ti-Ni (40-40-20)wt%, a high-quality layer on the substrate with good metallurgical bonding with minimal dilution is formed between the substrate and the coating, the microstructure of the clad layer depicts gray and white-colored fine structures. These revealed that the alloy TiC particles were dispersed in the matrix, as the Si element is confirmed from EDS analysis. It is known that Ti reacts with carbon and forms the TiC compound below 2350°C. The temperature generated during laser surface cladding leads to Ti and SiC particles dissolving in the melted pool thereby forms TiC compounds.

In the laser melted region, the coating and the substrate are heated to a temperature above the melting point and then rapidly re-solidified. The melting pool was mixed enough, gas and other impurities in the pool were thereby formed a fine layer. Besides, this ensured the quality of the layer. Figure 5 shows the cross-sectional SEM image of laser cladding of sample K1 at a scanning speed of 2 m/min and laser power of 2 kW. The significant increase in silicon carbide percentage and thus the alloyed layer is characterized by a significant number of pores and cracks. During sample preparation for metallographic study, alloyed layers have worn out due to porosity and brittleness.

The alloyed regions were found in some regions of a hard region. The hard regions were brittle and exhibited cracks due to stress generation. Thermal stresses have been developed due to high thermal gradients during cooling which originates crack. It is reduced by preheating the substrate.

The high degree of thermal expansion of the solidified clad materials and their substrate leads to cracking, as well as the delaminating of the clad from the substrate. There is no enough time for gas escape; a large number of pores and voids are due to low heat input and high cooling rate. The top region exhibits a small flower-like structure, just above the bottom of the alloyed laser region. Further, this indicates that the solidification starts with fine columnar grains from the bottom and ends with fine network grains.

3.4. XRD phase analysis for the first proportion

By comparing XRD and EDS results, particular phase formations in the laser-treated zone have been identified. The presence of unique chemical and physical metallurgical characteristics of the coating materials in the laser-generated melt region favors thermodynamic and dynamic conditions that form various phases by the reaction between the coating elements as well as the substrate.

The XRD spectrum of the laser clad layer of sample Q1 shown in Fig. 6. From the plane view samples of the clad, XRD spectra were taken. The spectra show the formation of Fe_3C, SiC, TiC, NiC, Si_5C_2, which ensures the mixing of coating material with the substrate, which is the reason for the good metallurgical bonding between clad layer and substrate. Thus partial decomposition of SiC into Si and C and. Mixing of the molten substrate and the preplaced material, mostly by convection, were observed by the Fe bearing phases detected during XRD analysis as well as the reasonably homogeneous microstructure were observed. Since SiC is excellent oxidation and creep resistance materials at high temperatures, the formation of its carbides widely applied in industries at solid-state as it strongly reacts with most transition metals and molten metallic substrate.

3.4.1. EDS analysis of sample Q1

EDS analysis of sample Q1 shown in Fig. 7. The white and gray particles in sample Q1, which exhibit high hardness lacking any pore or crack. The brighter region in the Q1 sample is found to have a large amount of Si and network grain region Fe, Ni predominantly. Silicon carbide phase was found in the Q1 sample that confirms the Si-rich zone. The other elements have been confirmed in XRD that indicate the presence of Fe and Ni-rich region γ-Fe and NiC phases comparing with the XRD analysis, sample K1 also exhibits the similar phases found in sample Q1.

3.4.2. EDS analysis of sample Q1

Figure 8 depicts the EDS analysis of specimen K1. Further, the EDS analysis of sample K1 shows that Fe, Ti, and Si were predominantly present. The laser-exposed area is predominantly reinforced with Ti and Si phases, which was shown by the above results. Thus the formed new phases increase the corrosion resistance and wear as exhibited in the EDS profile. In general, the retained austenitic phase due to Ni and Cr, corrosion resistance is evident.

5. Conclusions

This study concludes that by coating metal-ceramic powders (40% SiC-40% Ti-20% Ni) and ceramic powders (60% SiC-30% Ti-10% Ni) on SS316L specimen leads to increase surface hardness, excellent wear resistance, and high-temperature strength. With the help of optical microscopy, the microstructure of the MMC layers were studied, and it confirmed the grain refinement at the interface. The X-ray diffractometry, scanning electron microscopy results clearly confirmed that unfavorable hard ceramic particle on the MMC layer was found; this is attributed due to the formation of non-uniformity of coating thickness, crack formation at the layer of MMC, and microporous. The high hardness of the surface, elevated melting point, higher wear resistance, and high-temperature strength with low density was observed at reinforced laser-treated regions due to particle refinement with dispersion if hard SiC particle and precipitation of Cr_2C_3/Fe_2Si in the matrix, the improved wear resistance of laser clad material was observed. Utilizing advanced modeling and simulation technologies can improve the overall laser-based

phenomenon, which can be considered as the future work, driving forward the industry X.0 transformation.

Declarations

Acknowledgments

We would like to thank the Dr. Navalar Nedunchezhiyan College of Engineering, Cuddalore; Karpagam Academy of Higher Education, Coimbatore; Anna University, Regional Campus Madurai for completing this research work.

Declarations

The authors declare that they have no known competing financial interests or personal relationships that could have appeared to influence the work reported in this paper.

Funding

The authors did not receive support from any organization for the submitted work.

Conflicts of Interest

The authors declare that they have no conflict of interest.

Data Availability

The data used to support the findings of this study are included in the article.

Code availability

Not applicable.

Ethics approval and consent to participate

This chapter does not contain any studies with human participants or animals performed by any of the authors.

Consent for publication

This manuscript does not contain data from any individual person. Not applicable.

Authors' Contributions

Conceptualization: C. Ramesh Kannan, S. Manivannan; Methodology: C. Ramesh Kannan, S. Manivannan; Formal analysis and investigation: C. Ramesh Kannan, B. Stalin, C. Kailasanathan; Writing - original draft preparation: C. Ramesh Kannan, S. Manivannan; Writing - review and editing: B. Stalin, C. Kailasanathan; Funding acquisition: C. Ramesh Kannan; Resources: S. Manivannan; Supervision: B. Stalin

References

1. Sahasrabudhe H, Bose S, Bandyopadhyay A (2018) In: Jonathan Lawrence (ed) Advances in Laser Materials Processing, 2nd edn. Woodhead Publishing, pp. 507-539. https://doi.org/10.1016/B978-0-08-101252-9.00017-0.
2. Wu CL, Zhang S, Zhang CH, Zhang JB, Liu Y, Chen J (2019) Optics & Laser Technology 115:134-139. https://doi.org/10.1016/j.optlastec.2019.02.029
3. Guan D, He X, Zhang R, Li R, Qu X (2018) Vacuum 148:319-326. https://doi.org/10.1016/j.vacuum.2017.12.003
4. AlMangour B, Grzesiak D, Borkar T, Yang J-M (2018) Materials & Design 138:119-128. https://doi.org/10.1016/j.matdes.2017.10.039
5. Ellis M, Xiao DC, Lee C, Steen WM, Watkins KG, Brown WP (1995) J. Mater. Process. Technol. 52:55–67. https://doi.org/10.1016/0924-0136(94)01443-5
6. Zhang Z, Yu T, Kovacevic R (2017) Applied Surface Science 410:225-240. https://doi.org/10.1016/j.apsusc.2017.03.137
7. Kumar K, Zindani D, Paulo Davim J (2018) Advanced Machining and Manufacturing Processes, Springer, DOI: 10.1007/978-3-319-76075-9
8. Quiroz F, García-Castillo FA, Reyes-Osorio LA, Ávila-Cabrera A (2016) Finite Element Modeling of Friction Stir Spot Welding (FSSW) of Ti-6Al-4V: In International Materials Research Congress, Springer, Cham, pp. 119-128.
9. Srivastava D, Chang ITH, Loretto MH (2001) Intermetallics 9:1003-1013, https://doi.org/10.1016/S0966-9795(01)00063-2
10. Dutta Majumdar J, Pinkerton A, Liu Z, Manna I, Li L (2005) Applied Surface Science 247:320-327. https://doi.org/10.1016/j.apsusc.2005.01.039.
11. Wang F, Mei J, Jiang H, Wu X (2007) Materials Science and Engineering: A 445–446:461-466. https://doi.org/10.1016/j.msea.2006.09.093
12. Li Q, Song GM, Zhang YZ, Lei TC, Chen WZ (2003) Wear 254:222-229. https://doi.org/10.1016/S0043-1648(03)00007-3

13. Vreeling JA, Ocelík V, De Hosson JTM (2002) Acta Materialia 50:4913-4924. https://doi.org/10.1016/S1359-6454(02)00366-X
14. Majumdar J, Li L (2009) Metallurgical and Materials Transactions A 40:3001-3008. https://doi.org/10.1007/s11661-009-0018-8
15. Chen T, Wu F, Wang H, Liu D (2018) Metals 8:601. https://doi.org/10.3390/met8080601
16. Sadeh S, Gleason GH, Hatamleh MI, Sunny SF, Yu H, Malik AS, Qian D (2019) Metals 9:1196. https://doi.org/10.3390/met9111196
17. Sano T, Eimura T, Hirose A, Kawahito Y, Katayama S, Arakawa K, Masaki K, Shiro A, Shobu T, Sano Y (2019) Metals 9:1192. https://doi.org/10.3390/met9111192
18. Troiani E, Zavatta N (2019) Metals 9:728. https://doi.org/10.3390/met9070728
19. Kallien Z, Keller S, Ventzke V, Kashaev N, Klusemann B (2019) Metals 9:655. https://doi.org/10.3390/met9060655
20. Li Z., Yu G, He X, Li S, Zhao Y (2018) Metals 8:799. https://doi.org/10.3390/met8100799
21. Hernando I, Arrizubieta JI, Lamikiz A, Ukar E (2018) Metals 8:536. https://doi.org/10.3390/met8070536
22. Wu J, Zhang H, Feng Y, Luo B (2018) Metals 8:443. https://doi.org/10.3390/met8060443

Figures

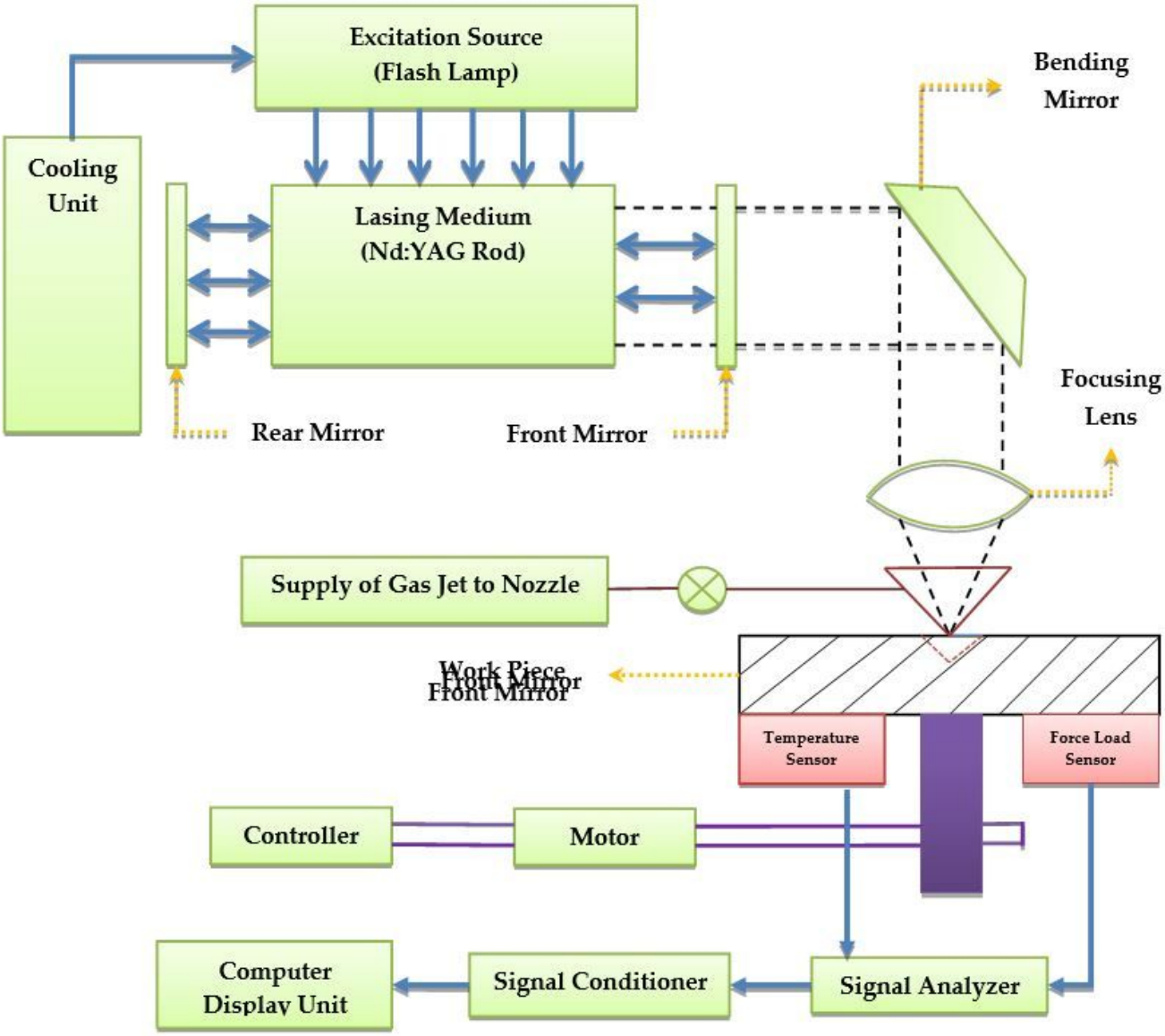

Figure 1

Experimental arrangement.

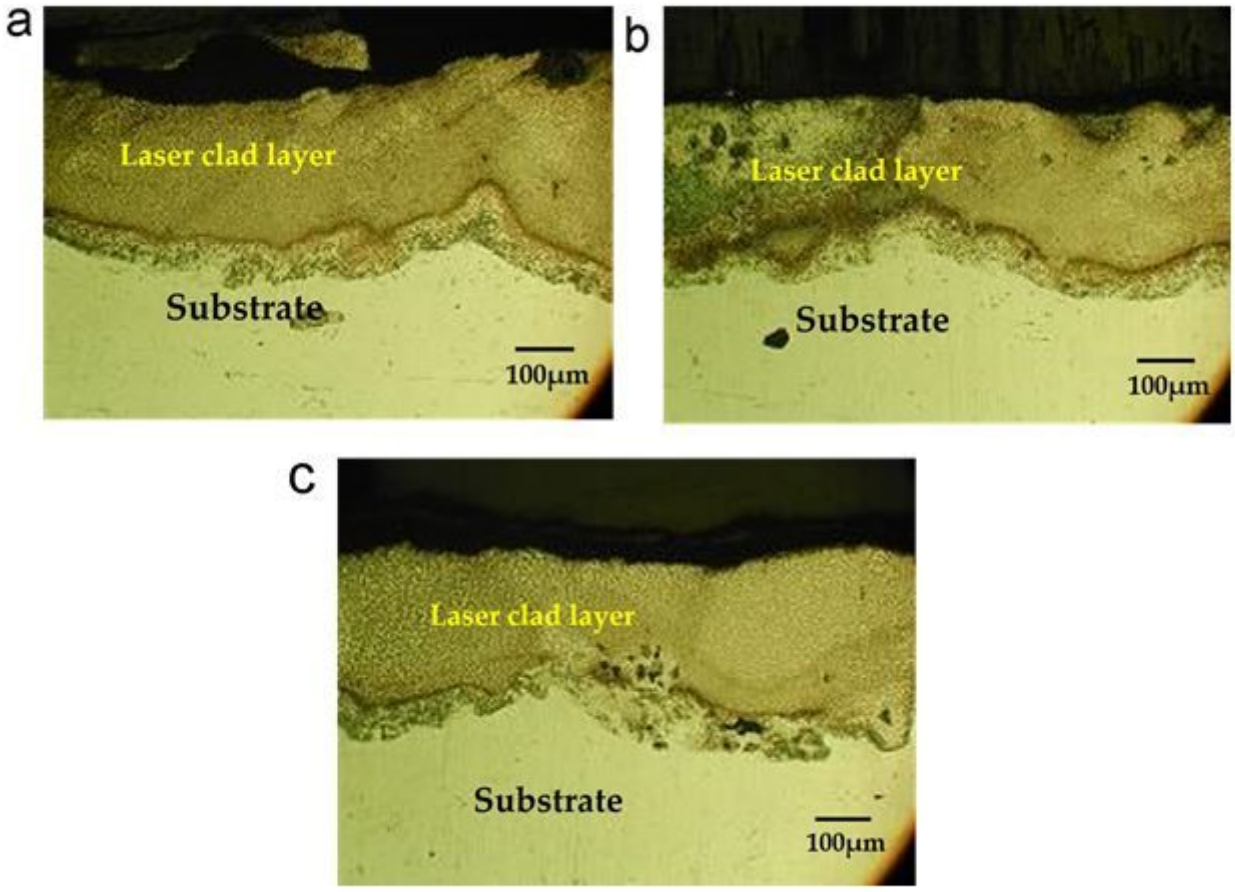

Figure 2

Microstructural image for cross-sectional view of (a) sample Q1 (192 microns) (b) sample Q2 (212 microns) and (c) sample Q3 (193 microns).

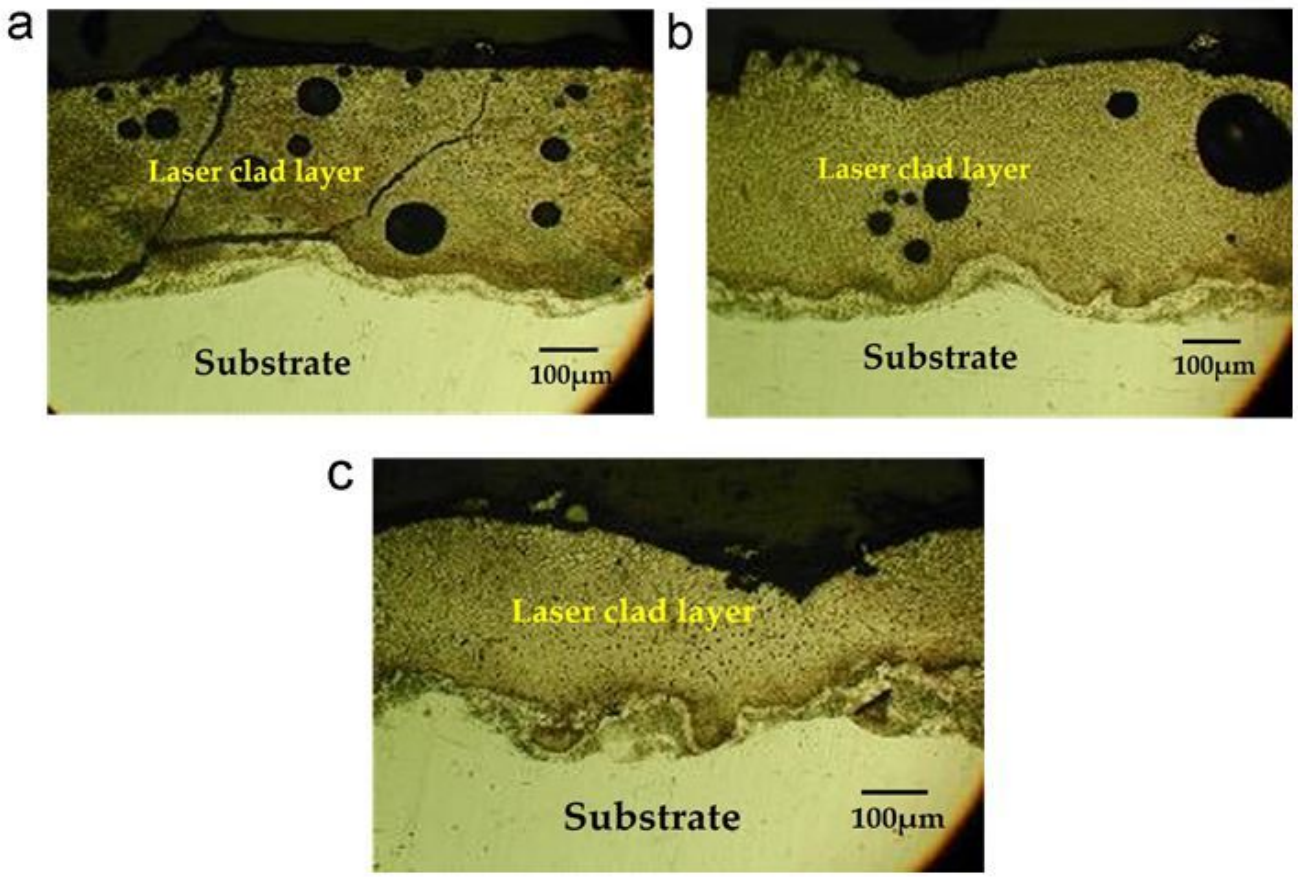

Figure 3

Microstructural image for cross-sectional view of (a) sample K1 (300 microns) (b) sample K2 (330 microns) and (c) sample K3 (276 microns).

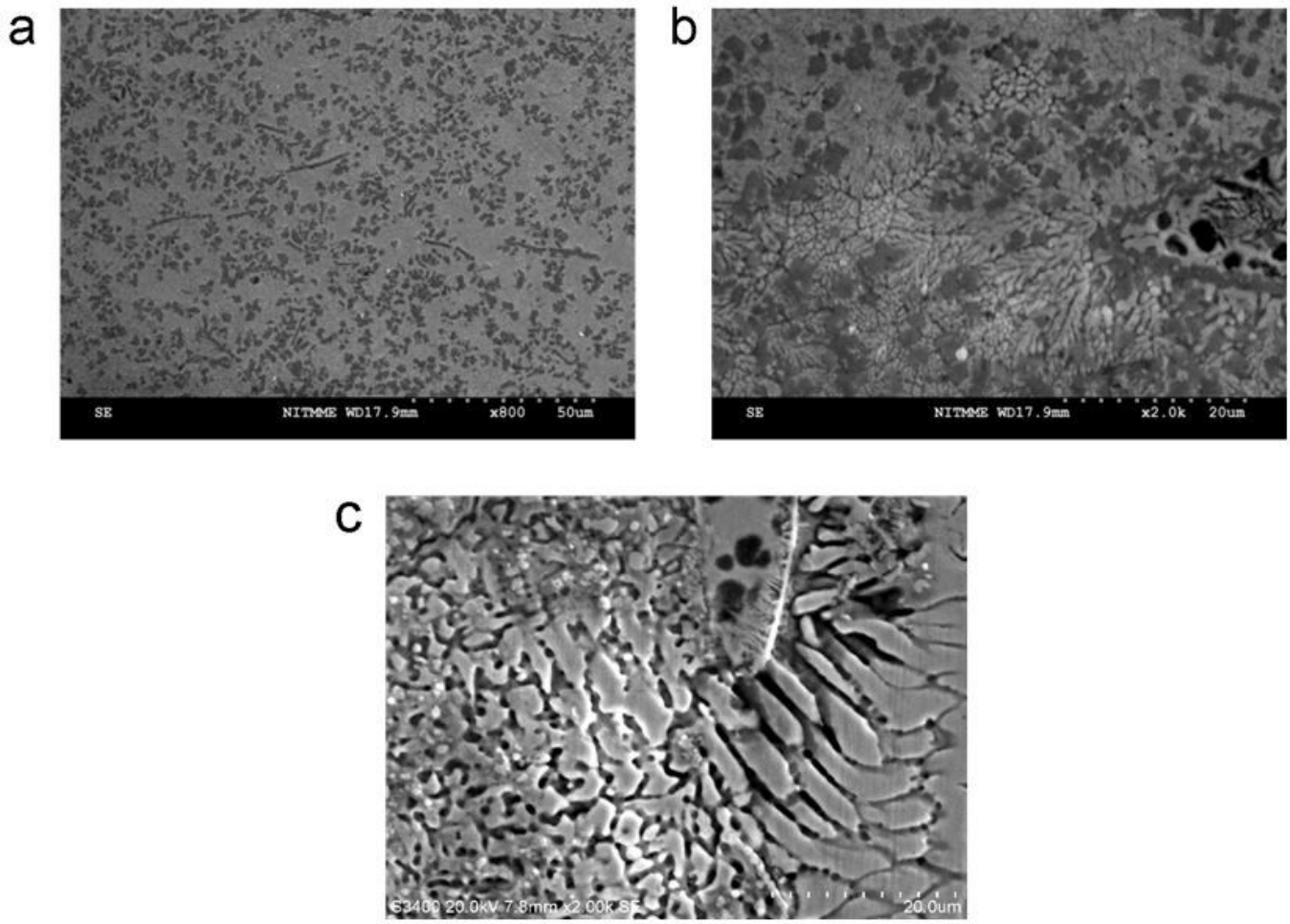

Figure 4

SEM image for the cross-sectional view of (a) specimen Q1 (b) & (c) specimen Q1 (interface).

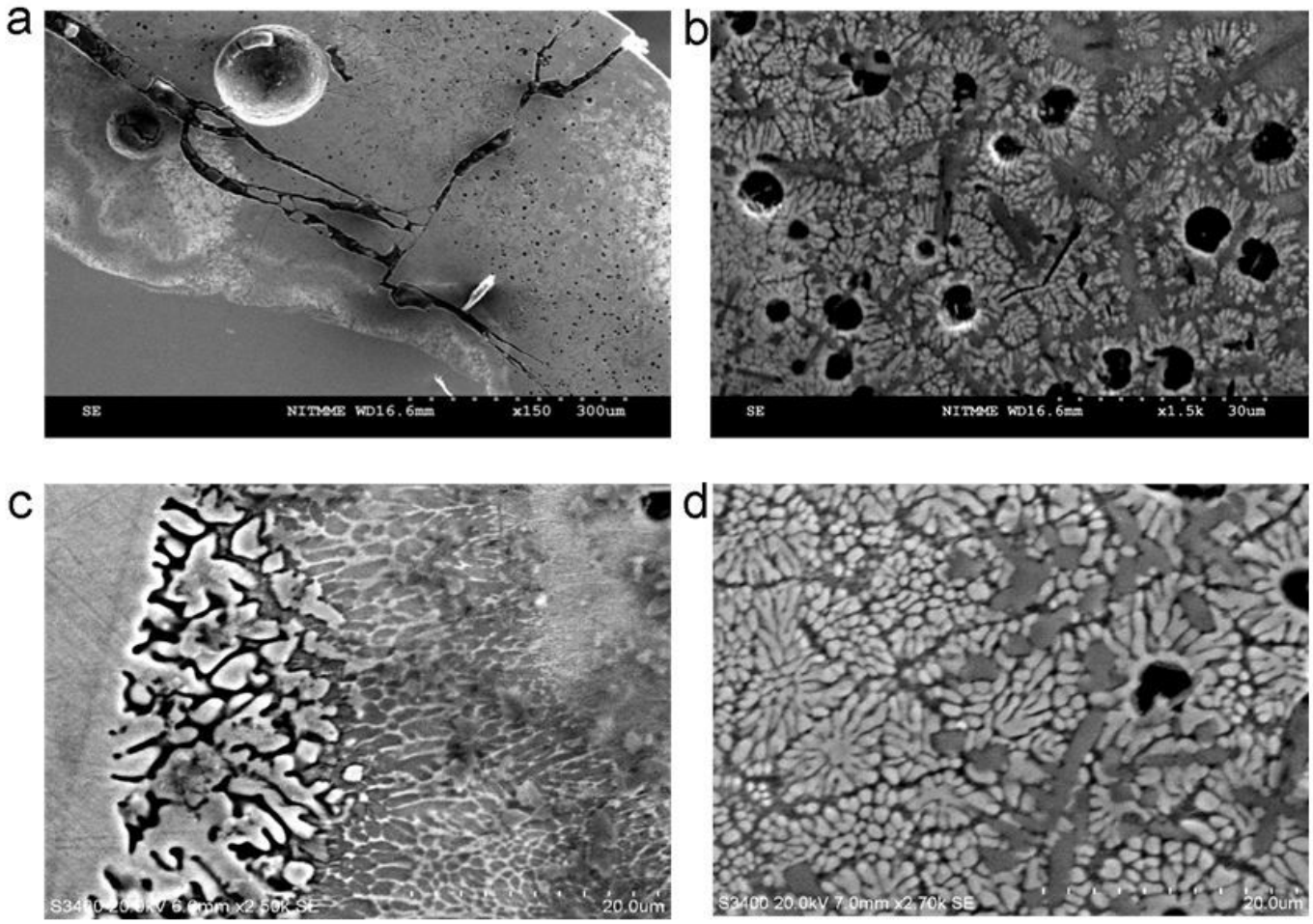

Figure 5

SEM image for the cross-sectional view of (a) & (b) specimen K1 (c) & (d) specimen K1 (interface).

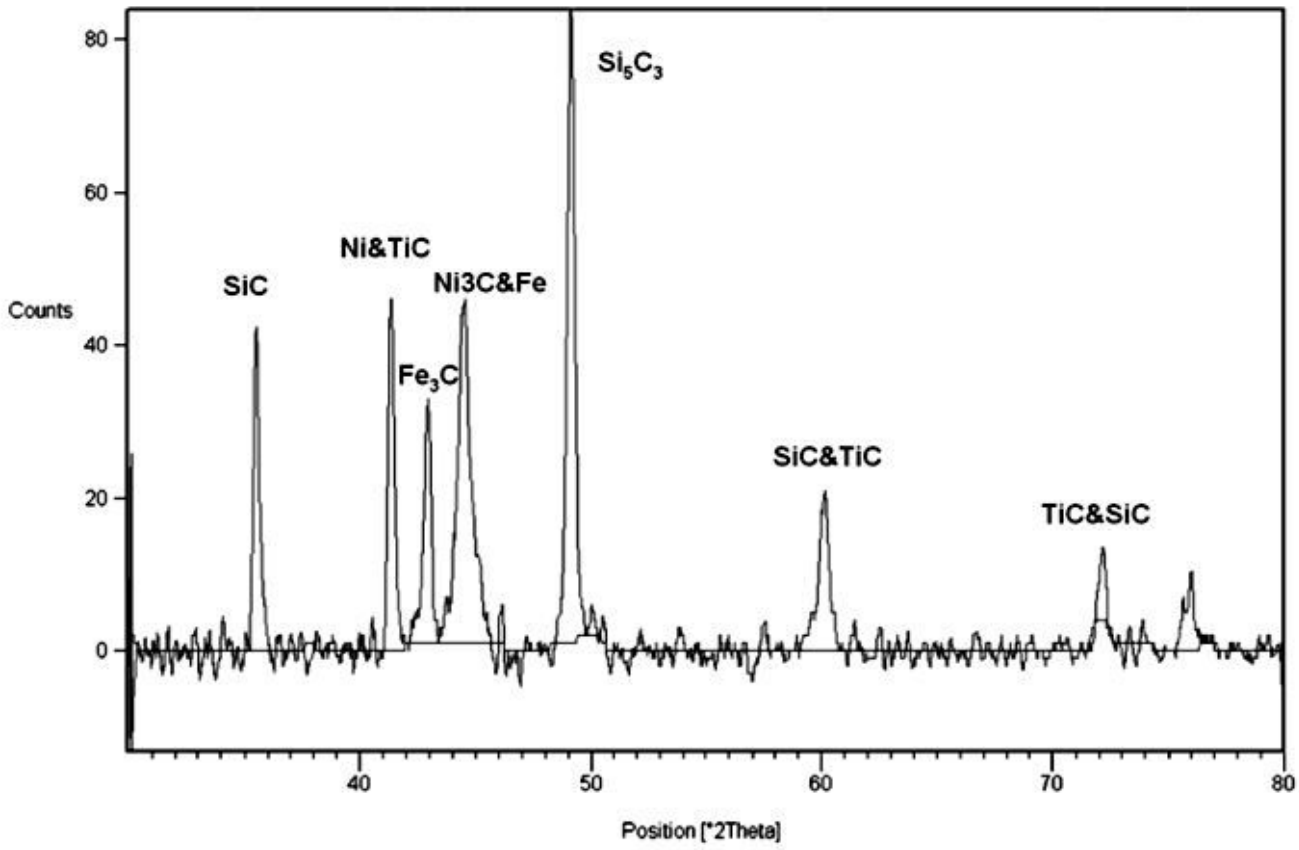

Figure 6

XRD spectrum of sample Q1.

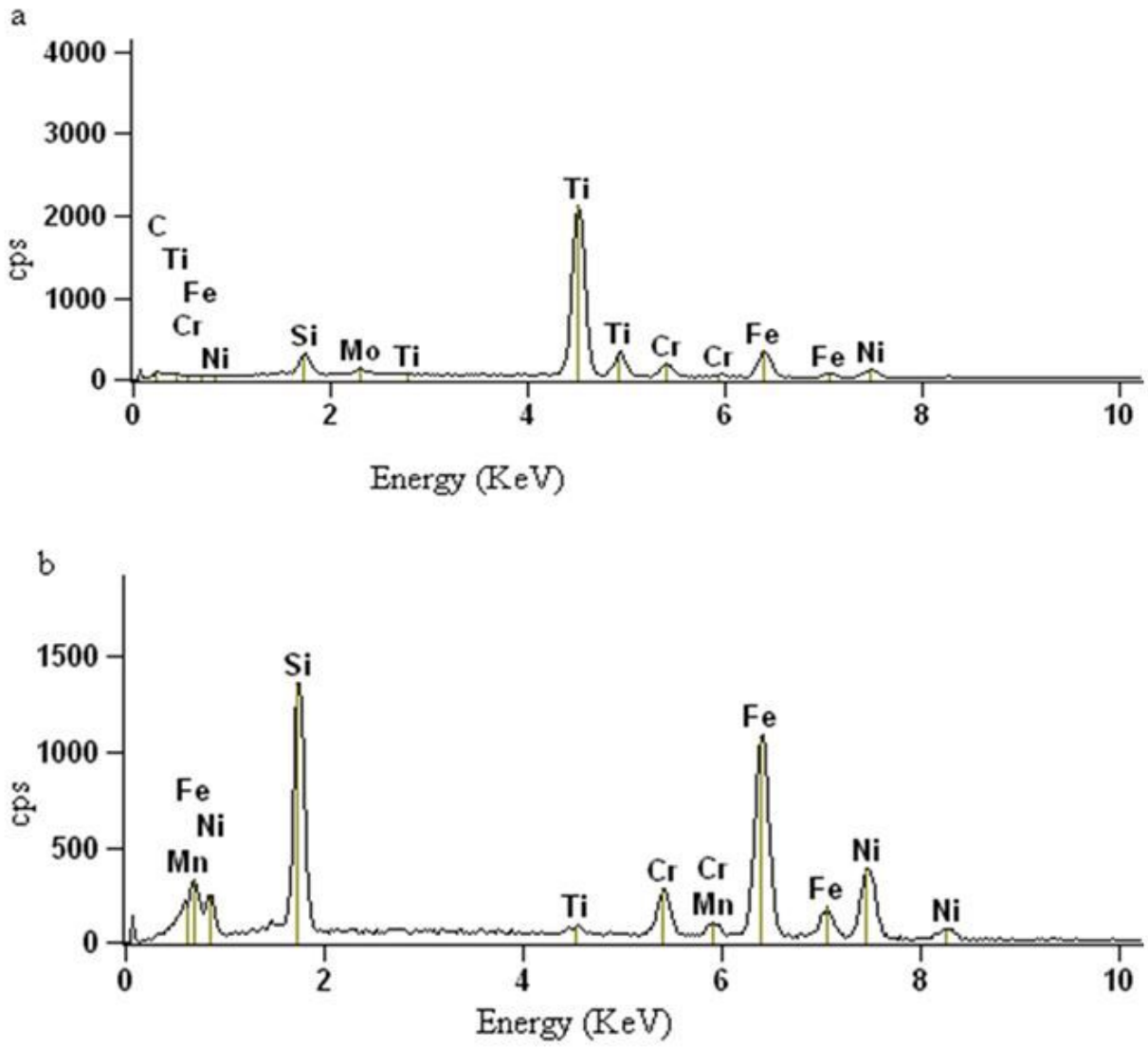

Figure 7

(a-b) EDS analysis of sample Q1.

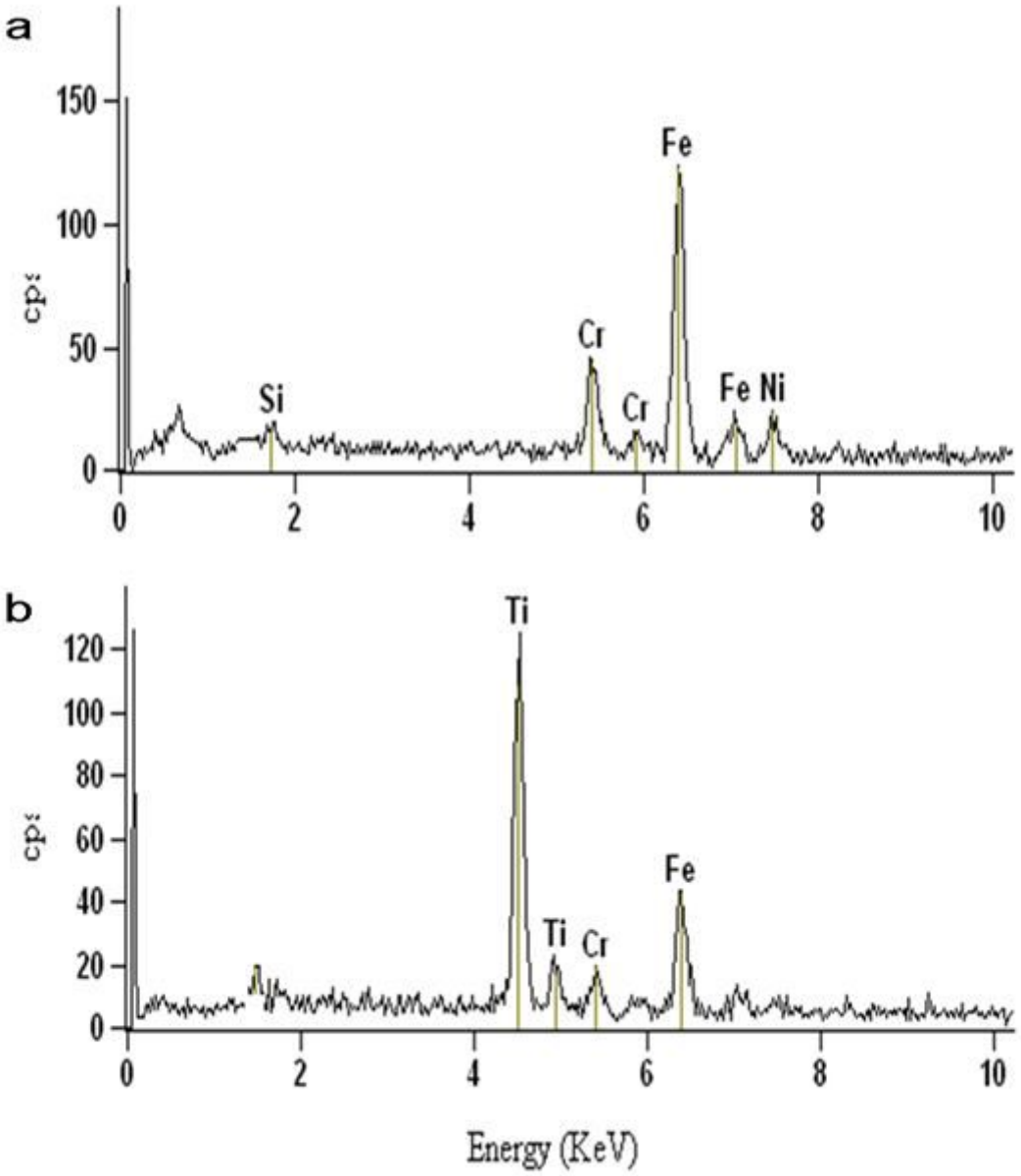

Figure 8

(a-b) EDS analysis of sample Q1.